Appl. Phys. B 76, 667–675 (2003)
DOI: 10.1007/s00340-003-1163-1

Applied Physics B
Lasers and Optics

CH. ANDREEVA[1]
G. BEVILACQUA[2]
V. BIANCALANA[2,✉]
S. CARTALEVA[1]
Y. DANCHEVA[1,2]
T. KARAULANOV[1]
C. MARINELLI[2]
E. MARIOTTI[2]
L. MOI[2]

Two-color coherent population trapping in a single Cs hyperfine transition, with application in magnetometry

[1] Institute of Electronics, BAS, Boul. Tsarigradsko Shosse 72, 1784 Sofia, Bulgaria
[2] INFM UdR Siena – Department of Physics, University of Siena, Via Roma 56, 53100 Siena, Italy

Received: 6 December 2002 / Revised version: 24 February 2003
Published online: 2 June 2003 • **© Springer-Verlag 2003**

ABSTRACT We investigate the coherent population trapping effect occurring between the Zeeman sublevels of a given hyperfine state of Cs when excited by a single-mode diode laser, which is frequency modulated in the kHz–MHz range. In the presence of a dc magnetic field, simultaneous excitation of pairs of ground-state magnetic sublevels to common excited magnetic sublevels is performed. As a result, coherent population trapping resonance is detected at only a given modulation frequency, whose value gives a measure of the magnetic field. The parameters of the resonances are measured in order to determine the ultimate accuracy of the magnetic field measurement.

PACS 07.55.Ge; 32.70.Jz; 42.50.Gy

1 Introduction

The coherent population trapping (CPT) effect has given rise to growing interest in the physics community since its first discovery in 1976 [1]. CPT usually appears as a decrease in the fluorescence signal when two coherent laser fields simultaneously excite two ground states to a common excited one (for a review, see for example [2]). CPT has been extensively studied in alkali atoms. CPT and related phenomena like electromagnetically induced transparency and electromagnetically induced absorption [3] have a very broad area of fundamental interests and applications in the fields of subrecoil laser cooling [4], steep dispersion [5], ultra-low group-velocity propagation [6], frequency standards [7], and many others. In application the interest is due to the very narrow spectral features of CPT and their sensitivity to external factors like dc electric field [8], electromagnetic field intensity and detuning (light shift), and magnetic field. We investigate CPT with the aim of application in the field of magnetometry.

As a general remark, it should be noted that all the results recently obtained in the field of CPT-based magnetometry have shown that these methods allow for measurement of magnetic fields with high accuracy and in a wide range of values. Moreover they have the practical and technical advantages of operating at room temperature and of being all-optical methods, so that substantially nonmagnetic sensors, coupled through optical fibers, can be built. The high accuracy comes from the fact that the magnetic field (MF) intensity is deduced by performing frequency measurements. MF measurements require many different criteria to be fulfilled at once. Geophysics, archaeology, and material science, for example, require compact, robust, and easy-to-operate devices for precise measurement and spatial mapping of MFs of moderate values (typical environmental values).

A further interesting feature of the CPT approach to magnetometry is that vector magnetometers can be built, with relatively high sensitivity and direction resolution.

Very interesting experimental results in the field of magnetometry have been recently obtained by Wynands and Nagel [9] using CPT prepared by two coherent laser beams exciting Zeeman sublevels belonging to the two different hyperfine (hf) ground states in Cs. Using a buffer-gas cell at relatively high pressures (of the order of 10 kPa), extremely narrow CPT resonances have been measured (full width at half maximum $\mathrm{FWHM}_{\min} = 42$ Hz), which set the sensitivity limit of the magnetometer to about $12\,\mathrm{pT}/\sqrt{\mathrm{Hz}}$, mainly due to the frequency noise of the laser source [10]. Comparable results have also been obtained in Rb as reported in [11]. The two hf ground states of Rb and Cs are separated by several GHz and the two laser frequencies can be produced either by phase locking two different laser sources [12] or by producing sidebands by means of direct diode laser (DL) modulation [13].

In both cases a bulky radio-frequency (rf) generator is necessary in the experimental setup, to generate a signal in the range of several GHz that matches (either directly or with a given harmonic) the frequency separation of the two ground states. From a practical point of view, it should be noted that it is an essential and nontrivial task to couple a substantial fraction of the GHz-range rf power into the DL in order to obtain a high modulation index at a reasonably low rf power.

The direct modulation approach has the advantage of being much more stable and reliable, and is commonly used at present. Nevertheless, it is worth noting that, in both cases, the final resolution is limited by the absolute uncertainty of the rf which, even having a frequency stability as good as 10^{-9}, can reach up to several Hz of absolute uncertainty. As a consequence very accurate measurements demand special attention to the accuracy and stability of the rf generator.

✉ Fax: +39-0577/23-4689, E-mail: biancalana@unisi.it

Another CPT-based technique which can be utilized for MF measurements has been recently developed [14]. In this approach CPT is established in degenerate systems, and specifically Λ chains are created when Zeeman sublevels of a single hf state are excited by two co-propagating laser beams with variable-frequency offset. In the presence of a dc MF a subnatural width resonance splitting is observed when the frequency offset is varied. The frequency offset at which the resonance occurs is a measure of the MF.

Similar results have been obtained in [15] where pure single-frequency excitation is used and thus the experimental setup is significantly simplified. The subnatural width resonances are observed when scanning the MF around zero. It has been shown that the width and the contrast of the observed resonances depend on the presence of the residual MF and this suggests the possibility of evaluating weak MFs by measuring such parameters. The general scheme of this latter approach has similarities and analogies with Hanle-effect experiments, as well as with measurements of the nonlinear Faraday effect (NLFE).

Remarkably narrow NLFE resonances have been measured ($\gamma \approx 2\pi \times 1.3$ Hz), the width of which is limited by the alignment relaxation in spin-exchange collisions [16]. Here it is worth noting that, in contrast to NLFE, which is related to the MF component along the light-propagation axis, the CPT signal is related to the modulus of the MF. This is due to the fact that CPT resonances occur in dependence on the splitting of the Zeeman sublevels regardless of the quantization axis (MF direction). The orientation of the MF with respect to the light polarization only acts on the CPT amplitude, which e.g. vanishes in the specific case when they are parallel. Due to this complementarity, the use of both NLFE and CPT can facilitate building of a vector magnetometer.

To our knowledge, the best results so far in the field of optical magnetometry have been obtained for optical pumping magnetometer using potassium, where a resolution better than $1.8\,\mathrm{f\,T}/\sqrt{\mathrm{Hz}}$ has been obtained [17]. Such a resolution derives from the fact that extremely narrow rf resonances have been obtained (FWHM less than 1 Hz) in a 15-cm spherical cell with paraffin coating. The authors have replaced the gas-discharge lamp with a laser in order to ensure one essential technical advantage: to couple the light source and the detector with the cell by means of fibers, thus reducing magnetic influence of the equipment. This kind of optical–rf double resonance has also found application in fundamental research in the testing of fundamental symmetries [18, 19].

The work described in this paper has common features with the CPT experiments made in both the nondegenerate and degenerate systems discussed above and summarizes the experimentally investigated parameters that are relevant for application. We use two coherent laser radiations (ω_1 and ω_2 in Fig. 1), which in the presence of a dc MF excite a pair of Zeeman sublevels belonging to a single hf ground state. This is why we call the approach presented the 'two-color CPT effect', as in the case of experiments using two different hf ground states for the Λ system preparation. The two ground sublevels have $\Delta m_F = 2$ (m_F is the magnetic quantum number) and are excited to one Zeeman sublevel of the excited state, creating the so-called Λ system. Multiple Λ systems can be excited, depending on the total angular momentum of the ground state, and thus Λ chains are created (see Fig. 1).

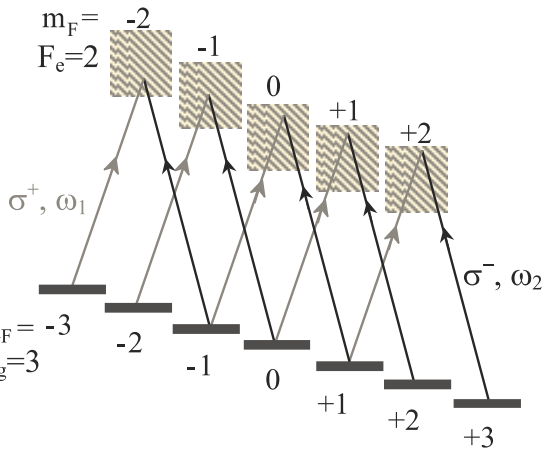

FIGURE 1 Λ systems in the $F_g = 3 \rightarrow F_e = 2$ transition created by the σ^+ and σ^- components of the respective frequencies ω_1 and ω_2, whose difference is equal to the splitting of the Zeeman sublevels with $\Delta m_F = 2$

It should be pointed out that, in our scheme, the two frequencies have a much smaller separation, the value of which depends only on the amplitude of the MF. Such a low-frequency modulation is a relevant advantage for practical application.

2 Level structure and Zeeman splitting of cesium hf ground states

The experiment is made by exciting transitions belonging to the D_2 line of Cs, where so-called cycling hf transitions are present, which give some advantages that are discussed later.

Let us introduce some general considerations about the level structure in Cs that are relevant to this application. Apart from specific values, most of these considerations apply to other alkali atoms as well and in particular to Rb, which is another good candidate for performing magnetometry experiments exploiting CPT.

In alkali atoms the energy splitting of the magnetic sublevels of the ground states is described by the Breit–Rabi formula, which gives a more precise evaluation with respect to the linear Zeeman description:

$$\nu_{m_F} = \frac{-\nu_{\mathrm{hf}}}{2(2I+1)} + g_I m_F B \frac{\mu_{\mathrm{B}}}{h} \pm \frac{\nu_{\mathrm{hf}}}{2}\sqrt{1+\left(\frac{4m_F}{2I+1}\right)x+x^2}\,, \tag{1}$$

where B is the MF intensity, x is given by

$$x = \frac{\mu_{\mathrm{B}}}{h\nu_{\mathrm{hf}}}\,(g_J - g_I)\,B\,, \tag{2}$$

and the values of the nuclear spin I, nuclear g-factor g_I, Bohr magneton μ_{B}/h, hyperfine frequency ν_{hf}, and fine-structure Landé factor g_J are reported in Table 1.

For small amplitude of the MF the Breit–Rabi formula, apart from constant terms, reduces substantially to the usual linear Zeeman effect, and the splitting of the magnetic levels

Data for ^{133}Cs $S_{1/2}$		
Nuclear spin I	7/2	
Nuclear g-factor g_I	−0.00039885395(52)	[20]
Bohr magneton μ_B/h	139.9624624(56) Hz/T	[21]
Hyperfine frequency ν_{hf}	9.192631770 GHz (exact)	[22]
Fine-structure		
Landé factor g_J	2.00254032(20)	[20]

TABLE 1 Cs data relevant for the Breit–Rabi formula

is approximately linear with the MF and proportional to m_F. It is interesting to evaluate the deviation from this behavior due to the nonlinear part of (1). With this aim, in Fig. 2 we report the deviation from linearity of the magnetically induced splitting between different pairs of Zeeman sublevels having $\Delta m_F = 2$.

The effect of this small nonlinear contribution, which makes the splitting between adjacent Zeeman sublevels slightly different, needs to be accurately discussed and analyzed. At very low MF amplitudes, when the linear Zeeman approximation applies, all the Λ systems arising from a given hf transition contribute simultaneously to enhancing a single CPT signal.

At intermediate fields, when the nonlinear terms in (1) are comparable with the line width of the CPT resonances, one observes significant broadening of the CPT spectral features, which would not be the case with measurements made by exciting both the ground hf states using GHz modulation.

At higher MF values, due to the nonlinear terms in (1), different Λ systems give resonances at different frequency separations of the two laser components, so that multiplets of subnatural width resonances can be resolved.

A Taylor expansion of the Breit–Rabi formula makes it possible to express the energy splitting between any pair of Zeeman sublevels having $\Delta m = 2$ in the form:

$$\delta\nu = \delta\nu_{\mathrm{LIN}} + \delta\nu_{\mathrm{NL}} \approx 2A'B - A''(m_{F,i+1} + m_{F,i-1})B^2, \qquad (3)$$

where

$$A' = \mu_0 g_F,$$
$$A'' = 2\frac{(\mu_B/h)^2\,(g_J - g_I)^2}{\nu_{hf}\,(2I+1)^2}, \qquad (4)$$

and g_F is the Landé factor of the given hf ground state.

In this paper we consider MF values at which splitting of the resonances corresponding to different Λ systems is not observed. The limit of this assumption depends on the frequency resolution and it can be derived from the plots reported in Fig. 2. The highest value of the applied MF amplitude is 0.15 mT and, according to the plots in Fig. 2, this corresponds to a maximum deviation of 720 Hz between the highest and lowest Λ systems of the transitions starting from $F_g = 4$.

As can be seen in Fig. 2, the nonlinear terms responsible for splitting of the Λ resonances are mainly quadratic in the mT range, and hence the Taylor expansion described in (3) applies. In particular, for Cs and for the two isotopes of Rb the values obtained from (4) for A'' are reported in Table 2, together with the A' values and with the ratios A'/A''.

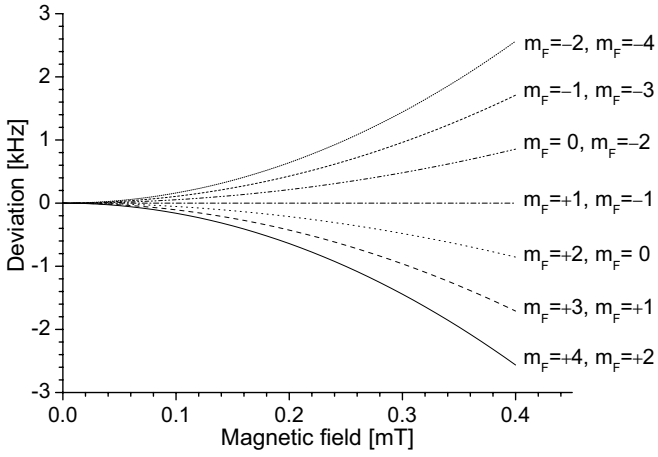

FIGURE 2 Frequency deviation of the two-photon resonances due to the nonlinear terms in the Breit–Rabi formula (1) as a function of the magnetic field for the $F_g = 4$ ground state of Cs. The plots represent the deviation from the linear (Zeeman) splitting between ground-state Zeeman sublevels separated by $\Delta m_F = 2$, like those participating in Λ systems. For the $F_g = 3$ case, the two extreme curves are to be neglected and the sign of the deviation is opposite

Element	F_g	A' (MHz/mT)	A'' (kHz/mT^2)	A'/A'' (mT)
Cs	3	3.5097	2.76	1300
	4	3.4986		
^{87}Rb	1	7.0236	14.4	486
	2	6.9958		
^{85}Rb	2, 3	4.66	14	330

TABLE 2 Coefficients of the linear and quadratic terms in the Taylor expansion of the Breit–Rabi formula

As can be inferred from the A'/A'' ratios, in the case of Cs the nonlinear behavior becomes relevant at a MF approximately three times larger, with respect to Rb.

3 Experimental setup and principle of operation

In this section the most important features and parameters of the experimental setup will be discussed as well as their influence on the ultimate accuracy in MF measurements. The experimental setup, presented in Fig. 3, consists of a frequency-modulated DL source, a sealed Cs absorption cell (diameter 3 cm and length in the range 1–6 cm, which can be with or without additional buffer gas), and a system for stray MF compensation/shielding and generation of a homogeneous dc MF.

3.1 *Magnetic field shielding and compensation*

The test measurements made in the laboratory to evaluate the final limits of our CPT approach to magnetometry were carried out under controlled conditions, and special care was needed to shield/compensate the stray MF, without introducing MF inhomogeneities. Two types of stray MF shielding/compensation were used.

The first uses high-permittivity material (μ-metal) to shield both dc and low-frequency MFs. We set up two concentric cylinders of CO-NETIC alloy, theoretically [23] attaining

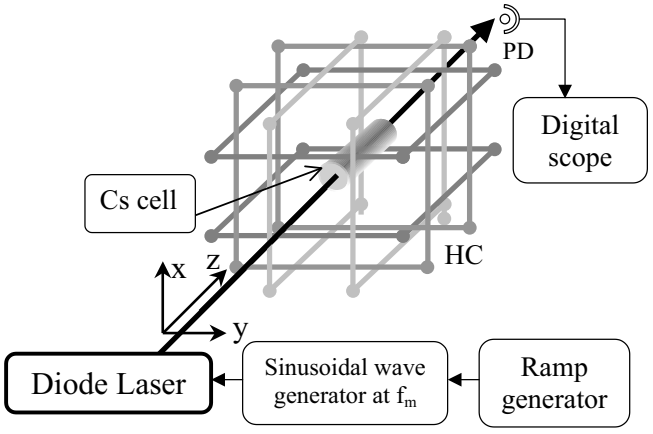

FIGURE 3 Experimental setup. HC is a set of three pairs of Helmholtz coils and PD is a photodiode. For some measurements, HC was replaced by μ-metal shielding

an extinction factor of 10^{-6} in our geometry. A homogeneous MF is applied longitudinally by means of a solenoid.

The other approach is based on three pairs of coils in a Helmholtz configuration to compensate the dc MF, together with a hollow aluminum cylinder to shield alternating MFs down to a frequency of about 20 Hz (thus attaining good extinction of the 50-Hz component) [24]. This configuration allows one to apply a controlled, modulated MF in any desired direction.

In the case of μ-metal shielding the gradients are mainly due to the finite size of the solenoid. Special care was taken and the final calculated homogeneity of the MF achieved ($\Delta B_{\text{long}}/B = 2 \times 10^{-5}$ on a 6-cm cell) was better than our experimental resolution.

In the case of Helmholtz compensation, assuming that the external stray fields are substantially homogeneous, we estimate the maximum spatial deviation as due to the finite sizes of the atomic sample and of the compensating coils, obtaining a relative $\Delta B_{\text{long}}/B = 1.2 \times 10^{-4}$ on a 6-cm cell.

For the purpose of having a compact experimental setup, the μ-metal shielding provides the best conditions to achieve very narrow resonances. On the other hand, the Helmholtz compensating system makes it possible to investigate the effects of MFs in different geometries, which is of particular interest for vector magnetometry and the study of polarization effects, with the disadvantage of a larger experimental setup.

3.2 *Laser source and CPT preparation*

As a light source we used a Mitsubishi single-mode DL emitting 850 nm at room temperature. High relative and absolute frequency stability of the DL was ensured by a highly stable current driver and precise temperature controller. We used a commercial (Newport) device, providing reliable stability and efficiency, apart from an unshielded rf noise (due to a broadcast emission at 1.5 MHz); minor harmful effects were also present, coming from the 50-Hz supply. The maximum output power available was of the order of 50 mW and the laser beam cross section was typically 0.08 cm^2. The DL operating in free-running regime had a line width of 45 MHz, which was measured using a beat signal between two identical DLs.

The presence of a MF removes the degeneracy between Zeeman sublevels of a given hf state. As stated above, a low-amplitude MF produces a separation between adjacent Zeeman sublevels that is proportional to the MF amplitude itself and is the same for all the pairs of adjacent Zeeman sublevels. Thus, in order to create Λ chains (as shown in Fig. 1), two coherent frequencies should be produced (ω_1 and ω_2 in Fig. 1) with a frequency separation twice the splitting of adjacent Zeeman sublevels (i.e. $\Delta\omega = \omega_1 - \omega_2 = 2A'B = 2\mu_B g_F B$). This resonance condition is simultaneously fulfilled for all the Λ systems, provided that the nonlinear deviation described in Fig. 2 is negligible. In the case of the D_2 line, according to the selection rules, each ground state is coupled to three different excited states. Nevertheless, we consider only the cycling transitions ($F_g = 3 \rightarrow F_e = 2$ and $F_g = 4 \rightarrow F_e = 5$) which, as discussed in [15], play the major role when a vacuum Cs cell is used.

The two coherent spectral components of the laser radiation are produced with controllable frequency separation by modulating the DL current. As mentioned in the Introduction, the difference in the Landé factors of the excited and ground states leads to slightly different resonance frequencies for different Λ systems. Nevertheless, due to both the atomic and the laser line widths, the whole set of Λ systems can be put in resonance simultaneously.

The rf modulation was introduced directly on the DL pins using a waveform generator whose frequency was in turn externally controlled. The external control made it possible to scan linearly the rf, as well as to introduce additional sine-wave modulation in order to make lock-in detection.

Due to the DL responses in frequency and amplitude, the rf signal causes both frequency and amplitude modulation, although the latter is negligible (less than 2% of amplitude modulation was measured using a fast photodiode). When the applied rf power was high enough to make the spectra detectable with Fabry–Perot interferometers, a perfectly symmetric frequency comb appeared that was consistent with pure frequency modulation.

Nevertheless, the effect of frequency-modulated laser light on atoms interacting with the beam for a short time (as in the case of Cs vapor in vacuum cells) can be identical to the case of amplitude modulation. The instantaneous frequency, as seen by the atoms of a given velocity class, while scanned over its range, goes periodically across the resonance.

3.3 *Evaluation of the modulation index through the CPT resonances*

In accordance with pure frequency modulation, we assume a spectrum composed of a number n of sidebands with respective amplitudes given by $J_n(m)$, where m is the modulation index. The actual spectrum of a frequency-modulated laser cannot be visualized directly by means of a Fabry–Perot interferometer when the modulation frequency is smaller than the laser line width. In this case, indirect evaluation of the modulation index can be made through the CPT effect.

The modulation index can be estimated through the number of the CPT resonances that are observed when the MF

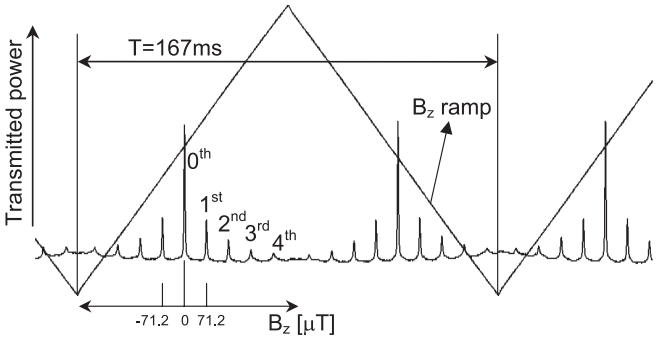

FIGURE 4 Transmitted light as a function of longitudinal magnetic field, obtained by exciting the three D_2 transitions starting from $F_g = 3$ with a laser field that is modulated with a fixed frequency of 500 kHz

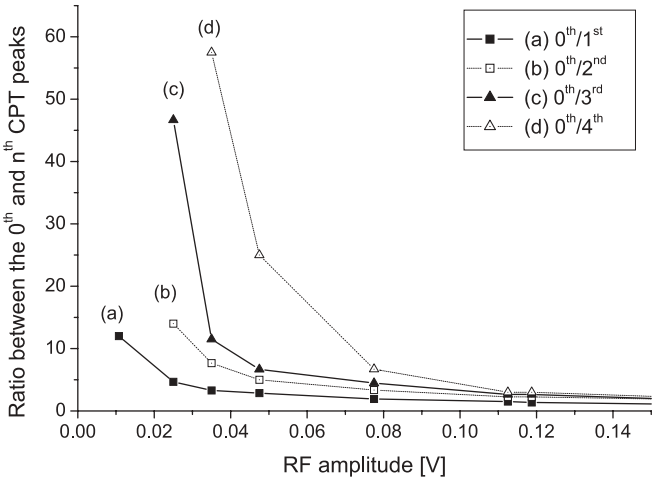

FIGURE 5 Ratios between the CPT at $B_z = 0$ (0th peak) and 1st CPT peak (curve (a)), 2nd-(b), 3rd-(c), and 4th-(d) are reported as a function of rf amplitude

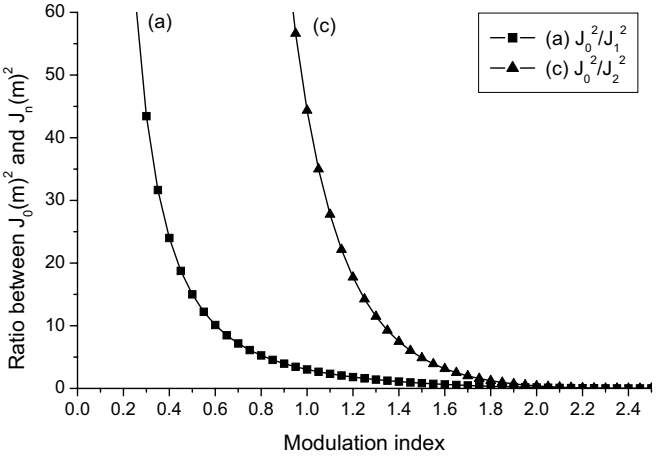

FIGURE 6 Ratios between the square of the 0th- and the 1st-order Bessel function (curve (a)) and of the 0th- and 2nd-order Bessel function (curve (b)), as a function of the modulation index m

is scanned at a fixed modulation frequency. One example of the signals recorded in these conditions is reported in Fig. 4, where the laser wavelength was tuned to the set of hf transitions starting from $F_g = 3$ and it was modulated at the fixed frequency $f_m = 500$ kHz (see Fig. 3). The beam was linearly polarized in the y direction. The transmitted power was measured with a photodiode and the signal was recorded by a digital oscilloscope. The MF was compensated in x and y directions, while the z component was scanned around the zero value by supplying the z Helmholtz coils with a low-frequency triangular signal. Thus, whenever the splitting of $\Delta m_F = 2$ sublevels of the ground state matched the frequency difference of a pair of the components of the DL spectrum, a Λ chain was created and a narrow CPT peak was observed.

In Fig. 4, besides the signal at $B_z = 0$ (0th peak), four pairs of CPT peaks appear. It can be inferred that sidebands with frequency separations of f_m, $2f_m$, $3f_m$, and $4f_m$ exist in the spectrum of the DL.

It is worth noting that the nth CPT peak is not in simple correspondence with the nth sideband, e.g. the 2nd CPT peak is due to the presence of the 0th and 2nd sidebands, but it may originate also due to the presence of 1st and -1st ones. The highest order of CPT peak gives information about the most distant pair of sidebands, having a suitably high power, and hence about the actual modulation index. For example, the existence of four orders of CPT peaks appearing in Fig. 4 indicates that the modulation index is large enough to provide sufficient energy in the $\pm$2nd sidebands.

For a given power density ($I = 0.68\,\mathrm{mW/cm^2}$ as a total power over carrier and all the sidebands) the ratios between the 0th CPT peak and each of the other CPT peaks were measured by changing the amplitude of the rf modulation at a fixed value of the rf frequency $f_m = 1$ MHz (see Fig. 5).

The modulation index can be estimated looking at Fig. 6 that shows the ratios between the square of the 0th- and the nth-order Bessel functions J_0^2/J_n^2, which represent the intensities of the corresponding sidebands. For the curve (a) in Fig. 5, the best coincidence between the ratio of the CPT peaks and the corresponding sideband ratio (curve (a) in Fig. 6) occurs at the beginning, when the modulation index is low enough ($m < 0.8$) and only the first sidebands contribute to the CPT signal. The same is valid for curves (c) and for $m < 1.5$ where the only relevant contribution to the CPT signal comes from the second sidebands coupled with the opposite first ones. Curve (b) cannot be considered, because the contribution from 1st and -1st sidebands cannot be distinguished from that of 0th and $\pm$2nd sidebands. Similarly the curve (d) does not have a nonambiguous interpretation.

It is important to note that no significant change of the amplitude of the already existing CPT resonances can be expected by increasing the modulation index, because of the complex contribution to the signal coming from all the sidebands. Actually, we can see from Fig. 5 that when increasing the rf amplitude by more than 0.1 V (which corresponds to a modulation index larger than 1.5) the amplitude of the 1st CPT peak does not increase and a stable maximum is being reached. This is why the experiments described later are performed at $m \approx 1.5$.

Signals like the one presented in Fig. 4 also make it possible to reflect on the nature of the CPT resonances produced in Λ chains. In the case of degenerate systems the excitation of the two independent Λ chains produces coherences between ground Zeeman sublevels which belong to two separate sets (with odd and even m_F values). In our case, even if the degeneration is removed, coherences between sublevels belonging to different Λs of a given chain can be expected. This hypoth-

esis is supported by the fact that throughout the range of MFs that we applied (up to several hundreds of μT) we did not observe significant differences between the shape of the 0th (degenerate case) peak and the other peaks (nondegenerate cases), as shown in Fig. 4.

4 Application to magnetometry

Let us discuss some of the most relevant parameters that influence the final absolute and relative accuracy of a magnetometer based on CPT.

The measurements discussed above concerning the evaluation of the modulation index are made by scanning the MF and keeping the rf constant. In contrast, the measurements for magnetometry are done by scanning the rf and keeping the MF constant. In such a condition, the 1st CPT peak occurs when the modulation frequency f_m equals $2A'B$ (see (3)).

The resonant f_m can be determined with an accuracy mainly depending on the line width of the CPT resonance and on the signal to noise (S/N) ratio. The absolute accuracy at this level is also determined by that of the rf generator, which makes this technique advantageous with respect to others based on GHz-range generators.

A non-negligible aspect of the problem is that the MF can be oriented in an arbitrary way in our coordinate system. This is why it is important to experimentally examine the features of the observed CPT peak, in particular its contrast and width, when a MF is present in different directions. A crucial point is to analyze how the behavior of these features depends on the field direction when different linear polarizations are used. This analysis is necessary in order to define a set of complementary measurements (with different light polarizations) that guarantee at least one large enough signal, regardless of the MF orientation.

4.1 *Excitation of the* $\mathbf{F_g = 3}$ *state*

A homogeneous dc MF was alternatively applied along the x, y, and z axes (see Fig. 3) and the contrast and width of the 1st CPT peak (when it existed) were measured depending on the input power density and on the laser-light polarization.

The DL frequency was tuned to the set of hf transitions starting from the $F_g = 3$ state and it was frequency modulated by means of direct DL current modulation using a sine-wave generator, whose frequency was slowly scanned in the interval from 200 kHz to 1.36 MHz. The slow triangular-wave scan of the rf modulation frequency was done at 6.17 Hz (see Fig. 7).

The transmitted signal was recorded using a digital oscilloscope and a typical signal is shown in Fig. 7, where the laser polarization is linear in the y direction and a dc MF is applied in the z direction.

Figure 8 represents the dependence of the 1 st CPT peak contrast on the laser power density, when linearly polarized (in the y direction) light is tuned to the maximum absorption of the group of lines starting from the $F_g = 3$ ground state. The contrast and width of the subnatural width resonance are measured by applying dc MFs in x and z directions. When the direction of the MF is parallel to the laser-light polarization (y direction) no CPT resonances are observed. It can be seen that,

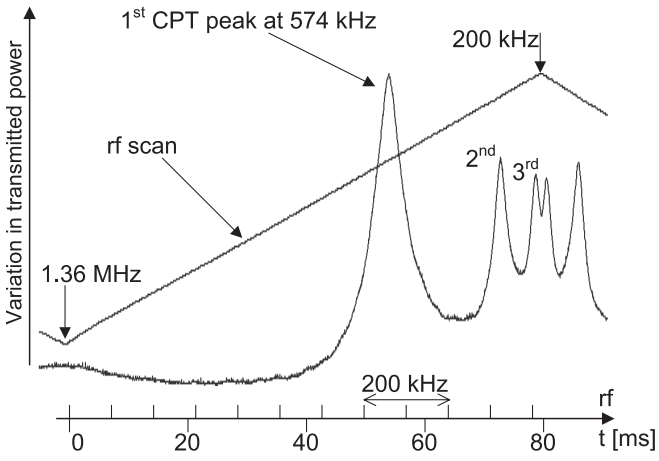

FIGURE 7 At a dc MF of 82 μT, scanning the rf, nonequally spaced peaks appear. Peaks are detected when either the rf or one of its harmonics satisfy the resonance condition. This happens at $f_m = 2A'B$ (for the 1st CPT peak), and at 1/2 and 1/3 of this value for the 2nd and 3rd CPT peaks respectively. The trace was obtained from the average of 16 traces to improve the S/N ratio, the resulting total measuring time being 2.6 s

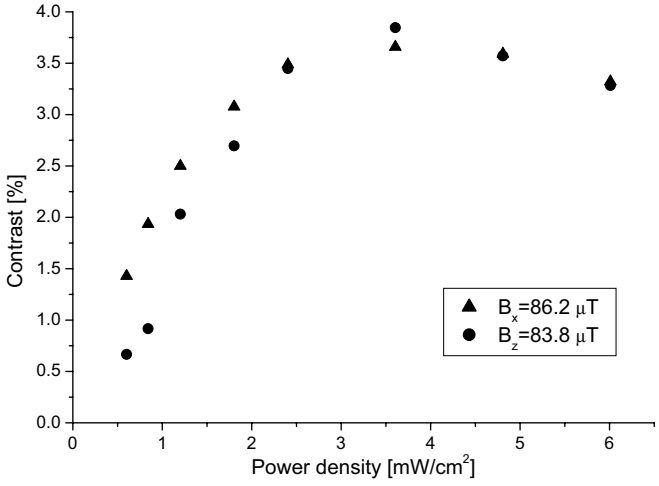

FIGURE 8 Contrast of the observed CPT structures as a function of the total power density, with a modulation index $m \approx 1.5$ and a beam size of 0.083 cm^2. The contrast is defined as the ratio between the 1st CPT peak and transmitted power out of the absorption line

when increasing the power density, the contrast of the 1st CPT peak increases and reaches its maximum value for total power densities greater than 2.5 mW/cm^2. However, the width of the CPT resonance also increases (see also [9, 15]). At power densities lower than 0.5 mW/cm^2, the CPT resonance width levels out at 37 kHz, which is attributed to the limited atom–light interaction time.

As noted above, the crucial parameters for precise MF measurements are the FWHM and the S/N ratio. As can be seen from Fig. 9, the lower the power density, the narrower the width of the resonance. However, Fig. 8 shows that the contrast of the feature drops dramatically (together with the S/N ratio) when the power density decreases.

In order to improve the S/N ratio and to evaluate the final resolution that one can obtain with this technique, we used an rf generator by driving it with a wide slow (55 mHz) ramp superimposed with a small and fast sine modulation (971 Hz). A lock-in detection referenced to the latter fre-

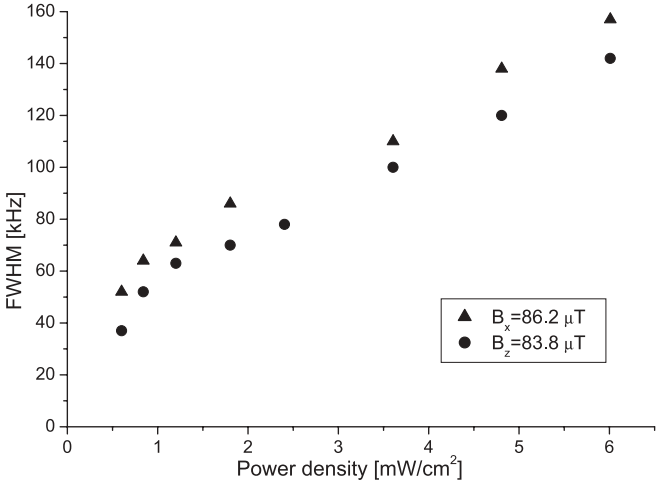

FIGURE 9 Width of the observed CPT structures as a function of the total power density, with a modulation index $m \approx 1.5$

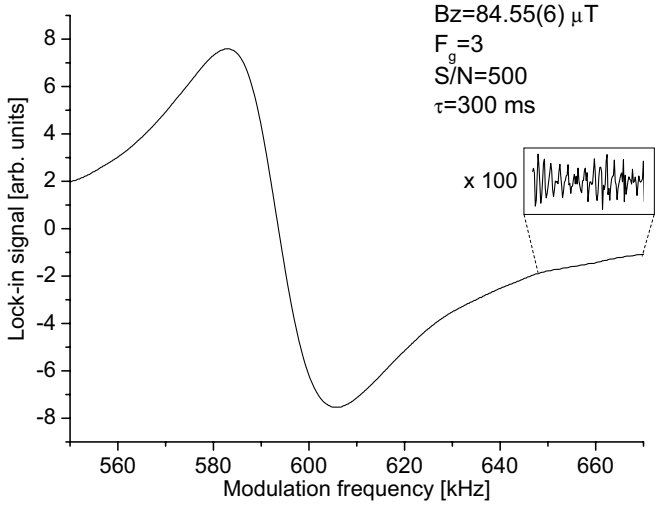

FIGURE 10 Signal from the lock-in amplifier as a function of the modulation frequency. A S/N ratio better than 500 has been achieved, allowing for 20-nT accuracy. The whole scan was recorded in 18 s

quency was used, obtaining signals like the one shown in Fig. 10.

As can be seen, the minimum FWHM obtained was still large, specifically of the order of 37 kHz. However the S/N ratio was significantly improved (S/N ratio better than 500). The zero crossing can be determined within an uncertainty of the order of 37 kHz/500, corresponding to an uncertainty of the order of 20 nT in the MF.

4.2 *Excitation of the* $F_g = 4$ *state*

When the laser frequency is tuned in resonance with the group of transitions starting from $F_g = 4$, a bright resonance is recorded in the fluorescence (this corresponds to a dip in the transmitted power) [15]. That result is obtained by irradiating the atomic sample with single-frequency, linearly polarized light.

In Fig. 11 is shown a typical spectrum of the transmitted light obtained when frequency-modulated, linearly polarized light was tuned to the maximum of the $F_g = 4$ group

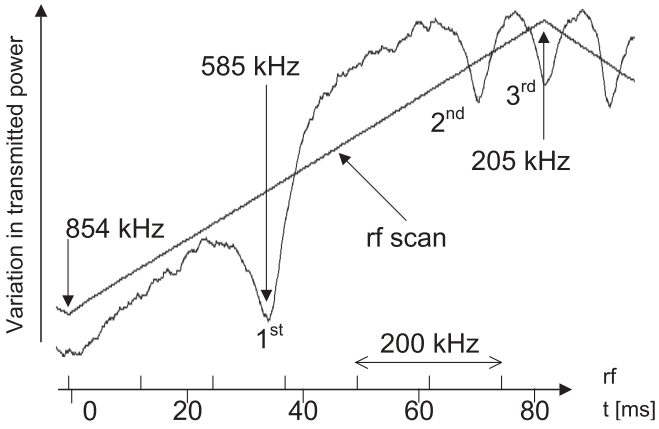

FIGURE 11 CPT dips observed when the laser is tuned to the set of lines starting from the $F_g = 4$ ground state and the modulation frequency is scanned in the presence of a dc magnetic field of 83.3 μT

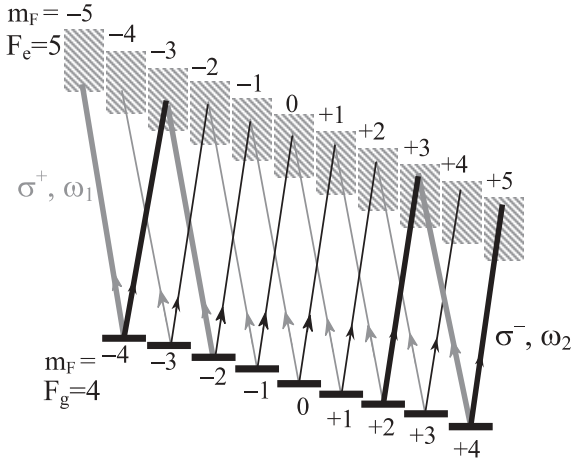

FIGURE 12 Interaction scheme in the case of the $F_g = 4 \rightarrow F_e = 5$ transition

of hf transitions in the D_2 line. A dc MF in the z direction was applied and the transmitted power was recorded in dependence on the modulation frequency. As can be seen a number of resonances appear, similar to the case of $F_g = 3$ (see Fig. 7). The interaction scheme can be represented as in Fig. 12, where the σ^+, ω_1 and σ^-, ω_2 excitations come from different sidebands having a frequency separation of $2A'B/i$, where $i = 1, 2, 3$, corresponding to the 1st, 2nd, and 3rd dips in Fig. 11.

It has been shown [25–28] that this kind of bright resonance can be attributed to constructive interference of atomic transitions. In [25] the authors show that, depending on the interaction scheme, both constructive and destructive interferences can be achieved and, in particular, constructive interference is possible when N-type systems are present which are sets of transitions involving two ground levels and two excited levels, like the ones represented with bold lines in Fig. 12. As expected from the theory developed in those papers, we observed resonances when the rf matched the splitting of the two ground Zeeman sublevels.

Regardless of the selected hf transition, the narrowest observed line width in vacuum cells is mainly determined by the interaction time of atoms with the laser field. Other possible

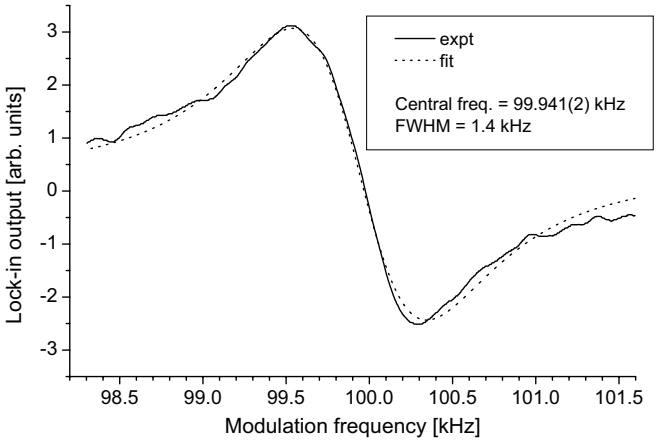

FIGURE 13 1st CPT peak recorded with lock-in detection, observed in lines starting from the $F_g = 3$ ground state, excited with linearly polarized light at a power of 64 μW and a spot size of 0.2 cm^2 with a 133-Pa Ar-buffered cell. The frequency modulation is swept in 3.6 s and the lock-in integration time is set at 30 ms. The *solid line* reports the experimental curve; the *dotted line* is the best fit obtained with the first derivative of a Lorentzian profile

factors that may broaden the line exist, such as fast jitter of the rf, scattered light, residual ac MF, and MF gradient (as discussed in Sect. 3).

4.3 *Measurements with a buffer-gas cell*

In order to reduce the broadening coming from the limited interaction time, the same experimental approach was applied using a Cs cell containing Ar at 133 Pa as a buffer gas.

In Fig. 13 we present the lock-in detected signal obtained by scanning the modulation frequency around the two-photon resonance corresponding to the 1st CPT peak in the case of Λ systems. As can be seen, a relevant (about 26-fold) reduction of the width was obtained due to the increased interaction time.

It is interesting to evaluate the accuracy with which the resonance frequency can be determined by numerical fits of the experimental data. As an example, in Fig. 13 a fitting curve is reported, modeled with the first derivative of a Lorentzian profile in addition to the experimental curve.

According to the results of the numerical fits, at the noise level of our present setup, this approach for measuring MFs of intermediate values gives a relative accuracy of the order of 2×10^{-5} evaluated according to the relative uncertainty with which the fitting procedure determines the center of the resonance. Further reduction of the line width and improvement of the S/N ratio will bring us to another limit set by the precision with which the value of A' is known. More precisely, looking at the numbers given in Table 1, it can be seen that a limit of 1.3×10^{-6} is set by the uncertainty of the value of the g_I Landé factor.

In addition to the limiting factors discussed above, a detailed investigation is needed in order to determine the influence of effects such as the resonant Stark effect (known as light shift), line distortion due to a nonuniform laser-light polarization, presence of ac magnetic fields which can produce line distortion and broadening, and many others.

5 Conclusions

In the present paper we have shown that subnatural width resonances are registered in the presence of a dc magnetic field when multi-frequency laser light excites the hf transitions starting from a given hf ground state of Cs. It has been shown that an increased absorption or transparency can be registered depending on the electromagnetically coupled ground state. We have illustrated the dependence of the coherent resonance parameters on the laser power density, magnetic field direction, and light–atom interaction time. Such resonances can be applied for measurement of MFs in the range of 10 μT–0.1 mT with a relative accuracy of 10^{-5} using the effect of CPT occurring at the Zeeman sublevels of a single hf ground state. This approach presents the possibility of significant size reduction and simplification of the experimental setup. Other advantages are that high precision in the magnetic field measurement is attainable with a lower relative stability in the radio frequency, the modulation frequencies are significantly reduced (down to the kHz or MHz range), and application to other atomic species is possible, regardless of the hf structure of their ground level. In order to make a more in-depth comparison between the previously developed methods using the CPT effect and the one presented here, further experimental investigations are necessary in order to determine the systematic errors and the ultimate accuracy.

As a general remark, it should be pointed out that the ultimate precision which can be reached with all the optical methods for magnetic field measurements is theoretically fixed by the peculiarities of the long-living levels involved. The use of an atomic medium as a magnetic field sensor provides us with a tool for absolute measurements where final precision is given by the knowledge of atomic constants without the need of calibration. All methods that use single ground hf state excitation will suffer a decrease in the signal amplitude due to unwanted population losses to the other ground state due to hf optical pumping.

The measured width of CPT resonances of 1.4 kHz makes it possible to measure magnetic fields in a wide range of values with an absolute accuracy of the order of 600 pT. Some of the resonance-broadening factors and limitations to final magnetic field measurement accuracy have been discussed.

ACKNOWLEDGEMENTS The authors are pleased to acknowledge the financial support of the European Union (Contract No. G6RD-CT-2001-00642) and the Bulgarian Science Fund (Grant No. F1005/00). They also wish to express their gratitude to E. Thorley for her help and assistance in preparing the manuscript and to S. Bartalini for his technical support.

REFERENCES

1 G. Alzetta, A. Gozzini, L. Moi, G. Orriols: Nuovo Cimento B **36**, 5 (1976)
2 E. Arimondo: Prog. Opt. **35**, 257 (1995) and references therein
3 S.E. Harris: Phys. Today **50**, 36 (1997)
4 A. Aspect, E. Arimondo, R. Kaiser, N. Vansteenkiste, C. Cohen-Tannoudji: Phys. Rev. Lett. **61**, 826 (1988)
5 S.E. Harris, J.E. Field, A. Kasapi: Phys. Rev. A **46**, R29 (1992)
6 L.V. Hau, S.E. Harris, Z. Dutton, C.H. Behroozi: Nature (Lond.) **397**, 594 (1999)
7 J. Kitching, S. Knappe, N. Vukicevic, L. Hollberg, R. Wynands, W. Weidemann: IEEE Trans. Instrum. Meas. **49**, 1313 (2000)

8 D. Budker, D.F. Kimball, S.M. Rochester, V.V. Yashchuk, M. Zolotorev: Phys. Rev. A **62**, 043 403 (2000)
9 R. Wynands, A. Nagel: Appl. Phys. B **68**, 1 (1999)
10 S. Brandt, A. Nagel, R. Wynands, D. Meschede: Phys. Rev. A **56**, R1063 (1997); M. Stähler, S. Knappe, C. Affolderbach, W. Kemp, R. Wynands: Europhys. Lett. **54**, 323 (2001)
11 M. Erhard, S. Nussmann, H. Helm: Phys. Rev. A **62**, 061 802 (2000)
12 M. Prevedelli, T. Freegarde, T. Hänsch: Appl. Phys. B **60**, S241 (1995)
13 C. Affolderbach, A. Nagel, S. Knappe, C. Jung, D. Wiedenmann, R. Wynands: Appl. Phys. B **70**, 407 (2000)
14 A.M. Akulshin, S. Barreiro, A. Lezama: Phys. Rev. A **57**, 2996 (1998)
15 C. Andreeva, S. Cartaleva, Y. Dancheva, V. Biancalana, A. Burchianti, C. Marinelli, E. Mariotti, L. Moi, K. Nasyrov: Phys. Rev. A **66**, 012 502 (2002)
16 D. Budker, V. Yashchuk, M. Zolotorev: Phys. Rev. Lett. **81**, 5788 (1998)
17 E.B. Alexandrov, M.V. Balabas, A.S. Pasgalev, A.K. Vershovskii, N.N. Yakobson: Laser Phys. **6**, 244 (1996)
18 K. Abdullah, C. Carlberg, E.D. Commins, H. Gould, S.B. Ross: Phys. Rev. Lett. **65**, 2347 (1990)
19 S.I. Kanorsky, S. Lang, S. Lücke, S.B. Ross, T.W. Hänsch, A. Weis: Phys. Rev. A **54**, R1010 (1996)
20 E. Arimondo, M. Inguscio, P. Violino: Rev. Mod. Phys. **49**, 31 (1977)
21 P.J. Mohr, B. Taylor: Rev. Mod. Phys. **72**, 351 (2000)
22 C.E. Tanner, C. Wieman: Phys. Rev. A **38**, 1616 (1988)
23 S.M. Freake, T.L. Thorp: Rev. Sci. Instrum. **42**, 1411 (1971)
24 The shielding effect of a conductive cylinder is due to Foucault (parasitic) current induced inside the metal. We measured the extinction factor of a longitudinal MF in our setup, where the aluminum hollow cylinder is 30 cm in length and has $R_{\rm int} = 5$ cm and $R_{\rm ext} = 8.5$ cm as internal and external radii, respectively. Such a device can be approximately described in terms of an RL circuit, where R is the resistance for tangential current and L is the inductance of a solenoid having the same size as the cylinder. A more accurate description of the conductor response to an axial oscillating MF can be made. The analytical solution of integral equations derived from Maxwell laws leads to an extinction factor at a frequency f given by $A(f) = B_{\rm int}/B_{\rm ext} = J_0(k_0 e^{i\pi/4} R_{\rm int}\sqrt{f})/J_0(k_0 e^{i\pi/4} R_{\rm ext}\sqrt{f})$, where $k_0 = \sqrt{2\pi\sigma\mu_0}$ depends on the conductivity σ. This approach also accurately reproduces the relative phase of the MF inside and outside the shield. At high frequencies ($f >> 1/(k_0^2 R_{\rm int}^2)$), an asymptotic value of the extinction factor can be found, and specifically $A(f) \approx \sqrt{R_{\rm ext}/R_{\rm int}}\exp[-k_0(R_{\rm ext} - R_{\rm int})\sqrt{f/2}]\exp[ik_0(R_{\rm ext} - R_{\rm int})\sqrt{f/2}]$, where the quantity $k_0\sqrt{f/2}$ appears, which is the inverse of the skin depth
25 C.Y. Ye, Y.V. Rostovtsev, A.S. Zibrov, Y.M. Golubev: Opt. Commun. **207**, 227 (2002)
26 A. Lezama, S. Barreiro, A.M. Akulshin: Phys. Rev. A **59**, 4732 (1999)
27 A. Lezama, S. Barreiro, A. Lipsich, A.M. Akulshin: Phys. Rev. A **61**, 013 801 (2000)
28 A. Lipsich, S. Barreiro, A.M. Akulshin, A. Lezama: Phys. Rev. A **61**, 053 803 (2000)